J. Fluid Mech. (1995), vol. 283, pp. 341–363

Inception of channelization and drainage basin formation: upstream-driven theory

By NORIHIRO IZUMI[1] AND GARY PARKER[2]

[1]Department of Civil Engineering, Tokyo Institute of Technology, 12-1 O-okayama 2 chome, Meguro, Tokyo 152, Japan

[2]St Anthony Falls Hydraulic Laboratory, Department of Civil and Mineral Engineering, University of Minnesota, Mississippi River at 3rd Avenue SE, Minneapolis, MN 55414, USA

(Received 20 December 1993 and in revised form 6 August 1994)

The ubiquitous presence of river drainage basins in the terrestrial environment suggests that distributed overland flow generated by rainfall tends to spontaneously organize itself into dendritic systems of discrete channels. Several recent numerical models describe the evolution of complete drainage basins from the initial condition of rainfall on a flat, tilted plateau, the surface of which has been provided with random elevation perturbations. These analyses model overland flow via the assumption of a perfect balance between gravitational and frictional terms, i.e. in terms of normal flow.

Linear stability analysis applied to the normal flow model has been shown, however, to fail to select a wavelength corresponding to a finite distance of separation between incipient basins. This suggests that the normal flow model may not be a sufficient basis for studying drainage basin development, especially at the finest scales of morphologic significance.

Here the concept of a threshold condition for bed erosion is combined with an analysis of the full equations of shallow overland flow in order to study wavelength selection. Classical linear stability analysis is shown to be inadequate to analyse the problem at the level of inception. An alternative linear analysis of bed perturbations based on the threshold condition is developed, and shown to lead to the selection of finite wavelength of the correct order of magnitude.

The analysis here is driven from the upstream direction in that bed erosion is first caused only when sufficient flow has gathered from upstream due to rainfall. A downstream-driven theory of incipient channelization that is not necessarily dependent upon rainfall is presented in Izumi (1993), and is presently in preparation for publication.

1. Introduction

Dendritic river drainage basins can be found everywhere on the terrestrial surface of the Earth where rainfall is sufficient. They constitute the dominant mechanism for the conveyance of rainwater to the oceans. The issue of their formation and structure has been of interest at least since the time of Horton (1945) and Strahler (1958). More recent work by Abrahams (1984), Sawai, Ashida & Imamoto (1986) and Howard (1990) is also of interest.

FIGURE 1. Map of the channel network (heavy solid lines), areas of thick colluvium (stippled area) and thick valley floor deposits of colluvium and alluvium (shaded area) near the headwaters of the Tennessee Valley drainage basin of Marin County, California. (Courtesy W. E. Dietrich; from Dietrich *et al.* 1993).

In the absence of dendritic networks of discrete streams, runoff resulting from rainfall would take the form of a very shallow, broad overland flow. The ubiquitous presence of such networks suggest, however, that overland flow over a flat, erodible tilted land surface is in some sense unstable over length scales beyond a given size. That is, it may be hypothesized that drainage basins are spontaneously self-organizing in a way that limits the scale over which unchannelized overland flow can occur.

The replacement of a full drainage basin with a flat, sloping surface, and the subsequent reinstatement of the drainage basin, can in general only be performed as a thought experiment. It is, however, possible to study the finest scales of existing drainage basins. The example of Tennessee Valley, California (Montgomery & Dietrich 1989), shown in figure 1, is of interest in this regard. The finest scale characterizing the basin itself appears to be the distance between first-order tributaries at their headwaters. This scale is seen to be of the order of 100 m. Montgomery & Dietrich (1989) have in fact found a mean spacing between heads of 82 m for the

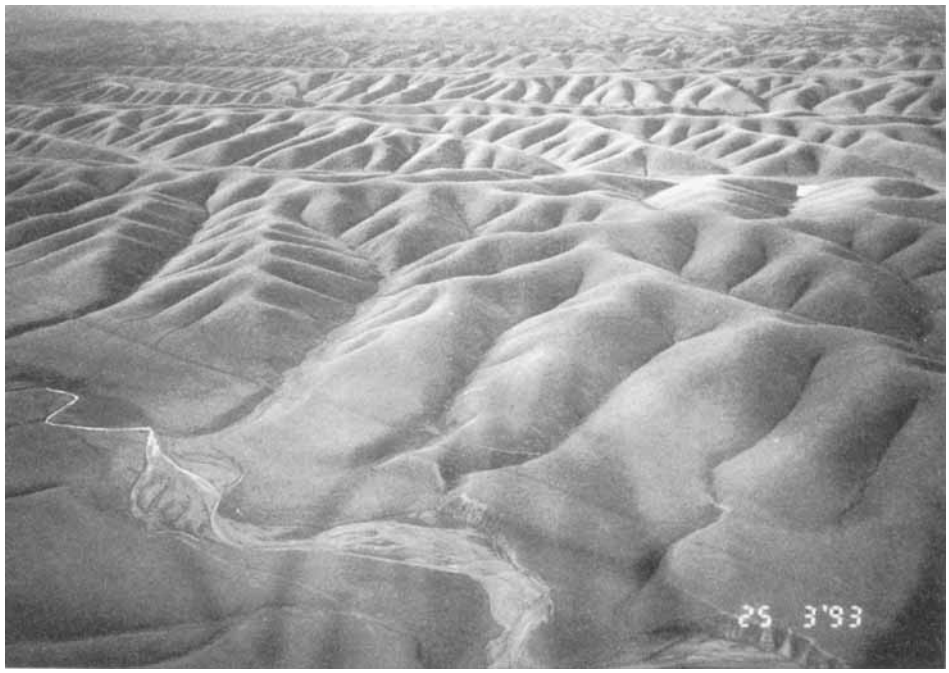

FIGURE 2. Rhythmic topography associated with channel heads on the east slopes of the Coast Range near Orland, California.

Hay Press tributary, and 81 m for the Sausalito tributary of the Tennessee Valley network. Dietrich & Dunne (1993) have found the following mean spacings between channel heads for three other river basins: Rock Creek, Oregon, 129 m; Southern Sierras, California, 110 m; and San Dimas, California, 64 m.

In a few cases, the topography associated with the headwaters of tributaries is particularly simple. An example is the topography along the east slope of the Coast Range of California near the town of Orland shown in figure 2. First-order tributaries are seen to run parallel to each other, each with its headwaters near a long divide running perpendicular to the channels. The spacing between adjacent headwater zones is again found to be of the order of 100 m. The rhythmic nature of the topography strongly suggests that the pattern of channels is the result of a flow–sediment interaction, the inception of which can be explained in terms of stability analysis.

A possible framework for such an analysis is shown in figure 3. A flat, tilted surface with slope S continues infinitely downstream of a divide. This surface is then provided with a transversely undulating topography of infinitesimal amplitude consisting of alternating troughs and ridges with an arbitrary wavelength of separation λ. The surface is subjected to rainfall and allowed to erode. The issue of interest, then is the selection of a characteristic wavelength of undulation, which would then provide a first estimate for the smallest characteristic scale of the drainage basin.

In recent years, it has become possible to model numerically the evolution of entire drainage basins. In the treatment of Roth & Siccardi (1989), for example, a flat, tilted surface is provided with random perturbations and subjected to rainfall. The resulting overland flow is modelled according to the normal flow hypothesis,

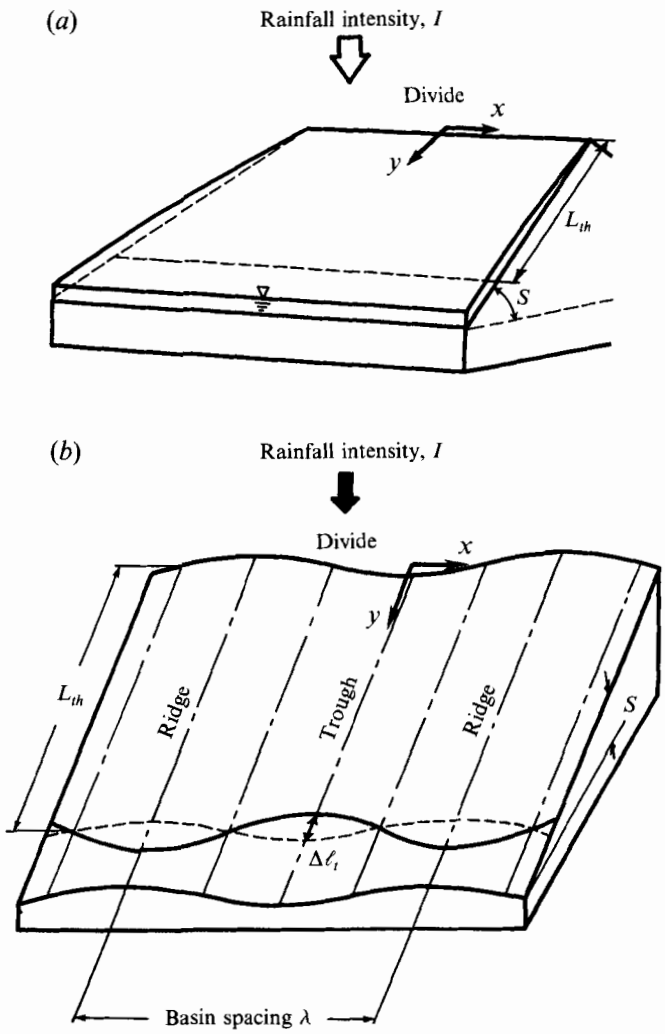

FIGURE 3. (*a*) Schematic diagram defining the base state. A flat but tilted plateau with slope S is subjected to a rainfall of intensity I (volume/area/time), which creates a sheet flow the intensity of which increases in the downstream (y) direction. The parameter L_{th} denotes the distance downstream of the divide at which the bed first starts to erode. (*b*) The base state is perturbed so as to render it wavy in the transverse (x) direction. The perturbation has wavelength λ. The dashed line denotes the line $y = L_{th}$. The adjacent solid line defines the distance downstream of the divide at which the threshold condition for bed erosion is reached in the presence of perturbations. Note that this distance is assumed to be shorter in the troughs than along the ridges. The parameter $\Delta\ell_t$ denotes the distance upstream of the point $y = L_{th}$ at which erosion first occurs in the troughs in the presence of the perturbations.

according to which the vector of flow resistance is in perfect balance with the vectorial force of gravity associated with the tilted topography. An appropriate relation for sediment transport is specified, and the bed is allowed to evolve in accordance with sediment continuity. When resulting topographic lows are connected in the downstream direction, the result has the distinct appearance of the early stages of drainage basin formation.

While the numerical model of Roth & Siccardi (1989) does not go beyond the early stages, that of Willgoose, Bras & Rodriguez-Iturbe (1989, 1991*a*, *b*) allows for the evolution of fully developed drainage basins in their entirety. They accomplish this by adapting a model for leaf vein formation to the problem. They treat the transition from unchannelized overland to channel in terms of an analogy to catalyzed chemical reactions (Meinhardt 1982). Their model of sediment transport is similar to that of Roth & Siccardi (1989) in that it is transportational in nature. Howard (1994) has responded to their inspiring work by devising a purely erosional treatment of overland flow with a minimum of assumptions, and in particular with no assumptions based on analogies to physically different problems. This model is also capable of evolving complex, realistic drainage basins.

All three of these numerical models rely on an initial tilted surface supplied with random perturbations, and treat the fluid phase in terms of simple normal flow. In one of the first theoretical treatments of the subject, however, Smith & Bretherton (1972) applied a linear stability analysis to the configuration of figure 3, and demonstrated that a transportational model based on normal flow is incapable of selecting finite wavelength. Rather, the dominant spacing tends to zero. Further work by Luke (1974) and Loewenherz (1991) confirms this result. Indeed, Loewenherz was obliged to introduce an *ad-hoc* 'smearing function' to prevent the tendency toward vanishing wavelength.

A question arises, then, as regards the finest scale appearing in any of these models. If the model itself has no inherent mechanism for scale selection, the fine scale may simply result from numerical diffusion acting on the arbitrarily specified spectrum of fluctuations of the initially randomized bed. The resulting drainage basin pattern is rendered dependent upon the initial perturbations and the size on the numerical grid of the computation.

The present treatment, then, is devoted to the issue of whether or not there is an inherent mechanism for wavelength selection that determines the finest scale of drainage basins. The reason for the failure of the normal flow model is elucidated, and the problem is resolved based upon a more general flow model.

2. The threshold concept

In recent years, the tools of linear and nonlinear stability analysis of erodible beds have been successfully used to determine the origin and characteristic of a variety of rhythmic morphologies, including dunes (Smith 1970; Engelund 1970; Fredsoe 1974; Richards 1980), alternate bars (Engelund & Skovgaard 1973; Parker 1976; Fredsoe 1978; Colombini, Seminara & Tubino 1987; Schielen, Doelman & de Swart 1993), and meanders (Ikeda, Parker & Sawai 1981; Blondeaux & Seminara 1985; Tubino & Seminara 1990).

These analyses allow the bed to deform and interact with the flow field in accordance with some slow time scale characterizing the rate of sediment transport. In a two-dimensional model of bed evolution, for example, the volume sediment transport rate per unit time per unit width is specified in terms of the vector (q_{sx}, q_{sy}); here y denotes the downslope direction and x the transverse direction in accordance with figure 3. This vector is taken to be a function of boundary shear stress and other parameters. Bed deformation is modelled using the Exner equation of sediment continuity:

$$\frac{\partial \eta}{\partial t} = -\frac{1}{1-\lambda_p}\left(\frac{\partial q_{sx}}{\partial x} + \frac{\partial q_{sy}}{\partial y}\right), \tag{2.1}$$

where η denotes bed elevation, t denotes time, and λ_p denotes bed porosity. The above relation is also used in Roth & Siccardi (1989) and Willgoose *et al.* (1989, 1991 *a, b*).

In the model of Howard (1994), however, overland flow is assumed to be purely erosional; all material eroded by the flow is allowed to be carried downstream without deposition. This concept is often used to treat the erosion of cohesive material. The rate of erosion normal to the bed E is specified as a function of boundary shear stress and other parameters. The Exner equation is then formulated as

$$\frac{\partial \eta}{\partial t} = -\frac{1}{1-\lambda_p} E. \tag{2.2}$$

Common to either of these formulations is the existence of a threshold parameter below which sediment transport of erosion does not occur. This is usually specified in terms of a threshold shear stress. In the erosional model, for example, E may be taken to be a function of the magnitude τ_b of the boundary shear stress vector (τ_{bx}, τ_{by}). A threshold shear stress τ_{th} may then be introduced such that E is a monotonically increasing function of τ_b for $\tau_b > \tau_{th}$, and E vanishes for $\tau_b < \tau_{th}$.

Montgomery & Dietrich (1989) have emphasized the role of at least three threshold parameters in the onset of channelization, one each for the processes of bed erosion by overland flow, daylighting of saturated groundwater flow, and mass movement. Here only the first of these is treated. Montgomery & Dietrich argue that overland flow over a vegetated, cohesive regolith has no chance of becoming channelized until it becomes intense enough to initiate the process of bed erosion. With this observation and the work of Howard (1994) as inspiration, a purely erosional model with a threshold shear stress is adopted here. It is furthermore specifically assumed that

$$E = \begin{cases} E(\tau_b), & \tau_b > \tau_{th}, \\ 0, & \tau_b \leqslant \tau_{th}. \end{cases} \tag{2.3}$$

Relations of this type are common in the literature on the erosion of cohesive sediment, e.g. Partherniades (1965) and Ariathurai & Arulanandan (1978).

The field work of Montgomery & Dietrich (1989), then, provides the conceptual basis for the present 'upstream driven' model: the rainfall-derived flow gathered from upstream of a point must be of sufficient magnitude to erode the bed if channelization is to start at that point. This concept can be expected to be valid for many but not all cases of incipient channelization. For example, the dendritic channel networks in tidal flats are likely formed from a point of lowered base level associated with low tide, which likely drives flow intensification and resultant incision. Rainfall is clearly not required for this process.

A problem with any model, erosional or transportational, which incorporates a threshold for bed deformation is that classical stability analysis becomes invalid in the vicinity of the point where the threshold condition is reached. This is because neither E nor the vector (q_x, q_y) is a smooth function of boundary shear stress in the vicinity of the threshold condition, so that neither is Taylor expandable. The idea is illustrated in figure 4, where τ_b is given as a function of transverse distance x at some distance y downstream of the divide in accordance with the bed perturbation of figure 3. Erosion is seen to be discontinuous, so disallowing the continuous perturbations characteristic of classical stability analysis.

Smith & Bretherton (1972) get around this problem simply by not introducing a threshold condition into their sediment transport relations. In some sense, then, their stability approach might be thought to be valid if downstream distance y is sufficiently large. In order to formulate this idea, consider the tilted surface in the

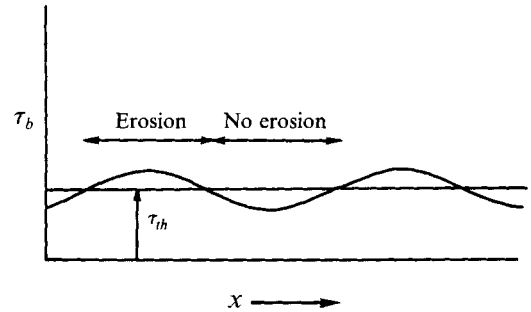

FIGURE 4. Diagram illustrating the transverse variation of boundary shear stress expected just downstream of the point $y = L_{th}$. Shear stress is above critical in some locations, but below critical in others, causing a discontinuous pattern of erosion. This feature renders the problem inappropriate for the methods of classical stability analysis.

absence of transverse perturbations of figure 3(*a*). Flow strength increases with y due to rainfall, so that the threshold for bed erosion is reached at $y = L_{th}$. The model of Smith & Bretherton, then, is valid for values of y sufficiently in excess of L_{th} that E becomes Taylor expandable everywhere.

If this same bed is perturbed by means of the transverse undulation of figure 3(*b*), flow will preferentially gather in the troughs, so that the threshold condition is attained slightly upstream of L_{th} in the troughs and slightly downstream in the ridges. It follows that channel formation should commence near $y = L_{th}$, and not at the larger distances at which the classical linear stability formulation of Smith & Bretherton (1972) might become valid. An alternative to classical linear stability analysis can thus be posed in the following form. Let $\Delta\ell_t$ denote the distance upstream of the point $y = L_{th}$ at which the threshold condition is attained in the troughs. In general, $\Delta\ell_t$ can be expected to be a function of wavelength λ, or wavenumber $k = 2\pi/\lambda$. At the linear level, the characteristic wavelength is here hypothesized to be the one such that erosion commences in the troughs in the shortest distance downstream of the divide. Minimizing this distance corresponds to maximizing $\Delta\ell_t$, so that the wavelength selection criterion becomes

$$\frac{\partial}{\partial k}\Delta\ell_t = 0. \tag{2.4}$$

The model of channelization implicit in this concept is illustrated in figure 5 . Channelization commences when the threshold condition is first overcome. The incipient channels can be expected to gather water farther downstream, thus intensifying the tendency for channelization. In addition, the point of first erosion can be expected to form an upstream-migrating head cut. The present analysis is 'upstream driven' only in the sense that sufficient water derived from rainfall must have been gathered by the catchment upstream of an incipient channel to actually cause bed erosion.

In order to simplify the analysis here, the transverse bed perturbation illustrated in figure 3(*b*) is assumed to be sinusoidal. Furthermore, the rainfall rate is assumed to be steady, corresponding to an extended steady precipitation event. Both these constraints could be relaxed in a more general treatment, but seem appropriate in the present first analysis.

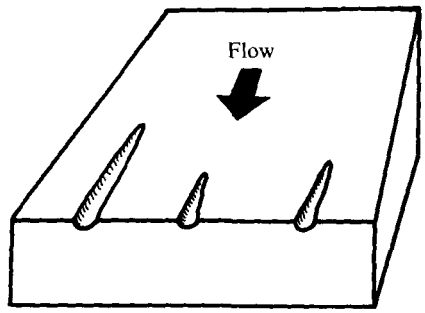

FIGURE 5. Expected pattern of incipient channelization resulting from the perturbation of figure 3(*b*).

3. Flow equations

In accordance with the usual quasi-steady assumption of erodible-bed flow problems, it is assumed that the setup time upon commencement of rainfall to achieve a steady flow is small compared to the time required for significant erosion to occur. The flow equations are thus approximated as steady.

Steady overland flow resulting from rainfall on a tilted plateau is thus considered. The depth-averaged St. Venant equations of shallow water flow provide an appropriate starting point for the analysis. The developed, dissected topographies of such existing basins as shown in figures 1 and 2 have relatively steep slopes near their headwaters. Here, however, the equations are applied to a hypothetical antecedent topography before dissection which has a relatively small slope, as described by figure 3. As shown in Izumi (1993), it is possible to include the Reynolds stresses associated with shear in the (x, y)-plane in an approximate way, so that the following equations result: streamwise momentum balance

$$u\frac{\partial v}{\partial x}+v\frac{\partial v}{\partial y}+g\frac{\partial h}{\partial y}=-g\frac{\partial \eta}{\partial y}-\frac{\tau_{by}}{\rho h}+\frac{\partial}{\partial x}\left(\nu_t\frac{\partial v}{\partial x}\right)+\frac{\partial}{\partial y}\left(\nu_t\frac{\partial v}{\partial y}\right), \tag{3.1}$$

transverse momentum balance

$$u\frac{\partial u}{\partial x}+v\frac{\partial u}{\partial y}+g\frac{\partial h}{\partial x}=-g\frac{\partial \eta}{\partial x}-\frac{\tau_{bx}}{\rho h}+\frac{\partial}{\partial x}\left(\nu_t\frac{\partial u}{\partial x}\right)+\frac{\partial}{\partial y}\left(\nu_t\frac{\partial u}{\partial y}\right), \tag{3.2}$$

and mass balance

$$\frac{\partial uh}{\partial x}+\frac{\partial vh}{\partial y}=I. \tag{3.3}$$

Here v denotes streamwise and u denotes transverse flow velocity, h denotes flow depth, I denotes the volume rainfall rate per unit time per unit bed area, here taken to be constant, (τ_{bx}, τ_{by}) denotes the vector of boundary shear stress, ν_t denotes the eddy viscosity associated with shear in the plane of flow, g denotes the acceleration due to gravity, and ρ denotes water density. The flow is assumed fully turbulent, so that boundary shear stress is given by the following relations:

$$\tau_{bx}=\rho C_f\left(u^2+v^2\right)^{1/2}u, \tag{3.4a}$$

$$\tau_{by}=\rho C_f\left(u^2+v^2\right)^{1/2}v, \tag{3.4b}$$

where C_f is a friction coefficient, here taken to be constant for simplicity. Eddy

viscosity ν_t is given as

$$\nu_t = \alpha u_* h, \tag{3.5}$$

where u_* denotes shear velocity, defined such that

$$\rho u_*^2 = \tau_b; \quad \tau_b = \left(\tau_{bx}^2 + \tau_{by}^2\right)^{1/2}. \tag{3.6a,b}$$

The parameter α in (3.5), although referring to momentum exchange, can be evaluated approximately with the aid of the literature on transverse mass exchange in channel flows, a summary of which can be found in Fischer *et al.* (1979). The information in Fischer *et al.* suggests values of α ranging from 0.1 to 0.3, in accordance with those used by Parker (1978) and Ikeda & Izumi (1991). Here the following simple approximation is used:

$$\alpha = 0.2. \tag{3.7}$$

The form of the bed perturbation illustrated in figure 3(*b*) can be expressed analytically as

$$\eta = \eta_d - Sy - a\cos kx, \tag{3.8}$$

where η_d denotes the (constant) unperturbed elevation of the divide, S denotes the unperturbed streamwise slope, a denotes the amplitude of the surface perturbation, here taken to be infinitesimal, and wavenumber $k = 2\pi/\lambda$, where λ is the wavelength of separation of the incipient channels. Note that (3.8) implies that the lines $x = 0, \pm 2\pi/k, \pm 4\pi/k, \cdots$ correspond to troughs. Substituting (3.4) and (3.8) into (3.1) and (3.2), it is found that the relations for momentum balance reduce to

$$u\frac{\partial v}{\partial x} + v\frac{\partial v}{\partial y} + g\frac{\partial h}{\partial y} = gS - C_f\frac{\left(u^2+v^2\right)^{1/2}}{h}v + \frac{\partial}{\partial x}\left(\nu_t\frac{\partial v}{\partial x}\right) + \frac{\partial}{\partial y}\left(\nu_t\frac{\partial v}{\partial y}\right) \tag{3.9}$$

and

$$u\frac{\partial u}{\partial x} + v\frac{\partial u}{\partial y} + g\frac{\partial h}{\partial x} = -gak\sin kx - C_f\frac{\left(u^2+v^2\right)^{1/2}}{h}u + \frac{\partial}{\partial x}\left(\nu_t\frac{\partial u}{\partial x}\right) + \frac{\partial}{\partial y}\left(\nu_t\frac{\partial u}{\partial y}\right). \tag{3.10}$$

One boundary condition on the flow is that the water discharge per unit width must vanish at the divide of figure 3,

$$vh\big|_{y=0} = 0. \tag{3.11}$$

If (3.3), (3.9), and (3.10) are to be solved on a domain that is infinite in x, the solution must be perforce cyclic in x. It follows, then, that transverse velocity must vanish at the ridges and troughs. Applied to the trough at $x = 0$, this yields

$$u\big|_{x=0} = 0. \tag{3.12}$$

Integrating (3.3) from ridge to ridge and applying the condition upon u at the ridges yields the compatibility relation

$$\frac{\mathrm{d}}{\mathrm{d}y}\int_{-\pi/k}^{\pi/k} vh\,\mathrm{d}x = \frac{2\pi}{k}I. \tag{3.13}$$

4. Base flow

The base flow is defined by the flow over the surface configuration of figure 3(*a*). It is obtained from (3.3), (3.9), and (3.10) by setting $a = 0$ and dropping all dependency

upon x, so that $u = 0$, $v = v_0(y)$, and $h = h_0(y)$, where

$$v_0 \frac{dv_0}{dy} + g\frac{dh_0}{dy} = gS - C_f \frac{v_0^2}{h_0} + \frac{d}{dy}\left(\nu_t \frac{dv_0}{dy}\right) \tag{4.1}$$

and

$$\frac{d}{dy}(v_0 h_0) = I. \tag{4.2}$$

An exact solution of (4.1) and (4.2) evidently requires one more boundary condition in addition to (3.11); this can be formulated in terms of vanishing Reynolds stress at the divide. It will be shown below, however, that it is not necessary to solve the equations for the base flow exactly. It suffices to start with the approximate base flow that results if the inertial and pressure terms, here called the backwater terms, and the Reynolds stress are dropped from (4.1). This flow is here termed the base normal flow, in that it represents a pure balance between the downstream gravitational force and the resisting force of bed friction.

The base normal flow resulting from these approximations satisfies (3.11), (4.2), and the approximate relation for momentum balance

$$0 = gS - C_f \frac{v_{bn}^2}{h_{bn}}, \tag{4.3}$$

where the subscript *bn* refers to the base normal approximation of the base flow. These equations can be solved to yield

$$v_{bn} = \left(\frac{gSI}{C_f}\right)^{1/3} y^{1/3} \tag{4.4}$$

and

$$h_{bn} = \left(\frac{C_f I^2}{gS}\right)^{1/3} y^{2/3}. \tag{4.5}$$

An interesting feature of the solution is that the Froude number F of the flow, given by

$$F^2 = \frac{v_{nb}^2}{g h_{bn}}, \tag{4.6a}$$

takes the constant value

$$F^2 = \frac{S}{C_f} \tag{4.6b}$$

in the case of the base normal flow. The analysis is seen to be equally valid for subcritical as well as supercritical flow in the Froude sense; the base normal solution passes through no obvious singularity in the vicinity of $F = 1$. The only restriction placed on F here is that it should not be larger than $O(1)$.

An *a posteriori* estimate of the neglected backwater and Reynolds stress terms can be obtained by substituting (4.4) and (4.5) into the appropriate terms in (4.1). This results in the estimates

$$v_{bn}\frac{dv_{bn}}{dy} + g\frac{dh_{bn}}{dy} \sim y^{-1/3}, \tag{4.7a}$$

$$\frac{d}{dy}\left(\nu_t \frac{dv_{bn}}{dy}\right) \sim y^{-2/3}. \tag{4.7b}$$

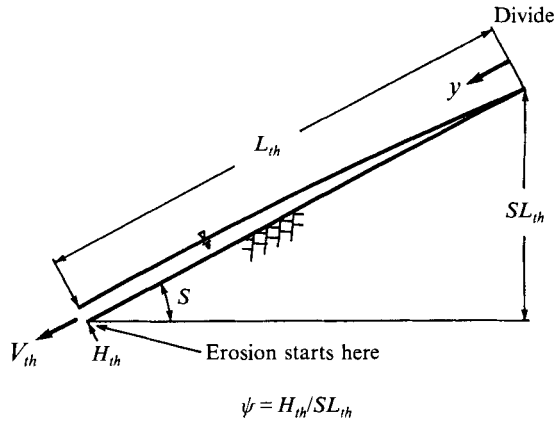

FIGURE 6. Definition diagram illustrating the following base state parameters: distance downstream of the divide L_{th} for the onset of bed erosion, flow depth H_{th} and velocity V_{th} at $y = L_{th}$, the elevation drop SL_{th} from the divide to the point of commencement of bed erosion, and the parameter ψ. Note that the slope has been exaggerated for clarity. This notwithstanding, the justification for the assumption of small ψ should be clear from the geometry.

The implication is that these terms are indeed small sufficiently far downstream of the divide. This result is placed on a more rigorous basis below.

The base normal flow can now be used to define the characteristic scales shown in figure 6. The streamwise flow velocity V_{th} at which the threshold condition is reached is found from (3.4) and (3.6) to satisfy the relation

$$\tau_{th} = \rho C_f V_{th}^2. \tag{4.8}$$

The momentum balance of the base normal flow, (4.3), requires that

$$C_f V_{th}^2 = g H_{th} S, \tag{4.9}$$

where H_{th} denotes the flow depth at threshold conditions. Finally, the distance L_{th} downstream of the divide at which the base normal flow reaches the threshold condition can be obtained by integrating (4.2):

$$V_{th} H_{th} = I L_{th}. \tag{4.10}$$

Once I, S, C_f, and τ_{th} are specified, (4.8)–(4.10) yield three relations for the three unknowns V_{th}, H_{th}, and L_{th}.

As can be seen from figure 6, the depth of the overland flow at threshold conditions H_{th} can be expected to be small compared to the elevation drop from the divide SL_{th} required to realize threshold conditions. A more detailed numerical illustration of this is presented later. The implication is that a parameter ψ can be defined such that

$$\psi = \frac{H_{th}}{SL_{th}} \ll 1. \tag{4.11}$$

5. Non-dimensionalization

The following normalizations are introduced:

$$(u, v) = V_{th}(\hat{u}, \hat{v}), \tag{5.1a}$$

$$(h, \eta, a) = H_{th}\left(\hat{h}, \hat{\eta}, \hat{a}\right), \tag{5.1b}$$

$$(x, y) = L_{th}(\hat{x}, \hat{y}), \tag{5.1c}$$

$$k = \frac{\hat{k}}{L_{th}}. \tag{5.1d}$$

Note that x, y, and k are made dimensionless in terms of L_{th}, and that $y = 1$ precisely when the dimensioned distance downstream of the divide is equal to L_{th}, at which the base normal flow attains the threshold for erosion. In addition, a transverse phase ϕ is introduced such that

$$kx = \hat{k}\hat{x} = \phi. \tag{5.2}$$

Several auxiliary dimensionless parameters will prove useful later. Let $\ell(x)$ denote the distance from the divide to a point where threshold conditions are reached. As shown in figure 6, the base normal value associated with this parameter is L_{th}. The deviation from this base normal value at any point x is defined in the following fashion:

$$\ell(x) = L_{th} - \Delta\ell(x). \tag{5.3}$$

As illustrated in figure 3(*b*), $\Delta\ell(x)$ is taken to be positive when $\ell(x)$ is less than L_{th}. The value of $\Delta\ell$ at the centre of a trough was defined previously as $\Delta\ell_t$. The above definition ensures that a minimum in ℓ is associated with a maximum in $\Delta\ell_t$. Dimensionless values of ℓ, $\Delta\ell$ (and thus $\Delta\ell_t$), and magnitude τ_b of the boundary shear stress vector are defined as follows:

$$(\ell, \Delta\ell) = L_{th}\left(\hat{\ell}, \Delta\hat{\ell}\right), \tag{5.4a}$$

$$\tau_b = \tau_{th}\hat{\tau}_b. \tag{5.4b}$$

After having introduced the above definitions, the hats are removed from the dimensionless forms for simplicity. With them, (3.9), (3.10), and (3.3) take the following respective dimensionless forms:

$$\psi F^2\left(ku\frac{\partial v}{\partial \phi} + v\frac{\partial v}{\partial y}\right) + \psi\frac{\partial h}{\partial y} = 1 - \frac{(u^2+v^2)^{1/2}}{h}v + \psi^2\epsilon\left[k^2\frac{\partial}{\partial\phi}\left(\chi\frac{\partial v}{\partial\phi}\right) + \frac{\partial}{\partial y}\left(\chi\frac{\partial v}{\partial y}\right)\right], \tag{5.5}$$

$$\psi F^2\left(ku\frac{\partial u}{\partial \phi} + v\frac{\partial u}{\partial y}\right) + \psi k\frac{\partial h}{\partial \phi} = -ak\sin\phi - \frac{(u^2+v^2)^{1/2}}{h}u + \psi^2\epsilon\left[k^2\frac{\partial}{\partial\phi}\left(\chi\frac{\partial u}{\partial\phi}\right) + \frac{\partial}{\partial y}\left(\chi\frac{\partial u}{\partial y}\right)\right], \tag{5.6}$$

$$k\frac{\partial uh}{\partial\phi} + \frac{\partial vh}{\partial y} = 1, \tag{5.7}$$

where

$$\chi = (u^2+v^2)^{1/2}h. \tag{5.8}$$

The parameter ϵ in the first two of these equations serves to scale the Reynolds stress terms; it is given by

$$\epsilon = \frac{\alpha}{C_f^{1/2}}S^2. \tag{5.9}$$

For thin overland flow over a vegetated surface, $C_f^{1/2}$ can be expected to be of the order of 0.1 (e.g. Yoon & Wenzel 1971; Shen & Li 1973). Using the estimate of α of (3.7), it is seen that ϵ scales as S^2, so that it is a small parameter in addition to ψ, i.e.

$$\epsilon \ll 1. \tag{5.10}$$

Equations (3.11)–(3.13) take the dimensionless forms

$$vh\big|_{y=0} = 0, \tag{5.11a}$$

$$u\big|_{\phi=0} = 0, \tag{5.11b}$$

$$\frac{\mathrm{d}}{\mathrm{d}y}\int_{-\pi}^{\pi} vh\,\mathrm{d}\phi = 2\pi. \tag{5.11c}$$

Equation (5.3) takes the dimensionless form

$$\ell = 1 - \Delta\ell. \tag{5.12}$$

Equations (3.4), (3.6), (5.1), and (5.4) can be used to obtain the following dimensionless form for the magnitude of the boundary shear stress vector:

$$\tau_b = u^2 + v^2. \tag{5.13}$$

It is seen that in general the threshold condition $\tau_b = 1$ is reached at the value $y = \ell$, where ℓ is defined by the relation

$$\left(u^2 + v^2\right)\Big|_{y=\ell} = 1. \tag{5.14}$$

This relation will later be used to determine characteristic wavenumber.

6. Normal flow analysis

The reason for the failure of the normal flow approximation used by Smith & Bretherton (1972) and others to select a finite wavelength can now be explained. This is first done in a linear context, and then in terms of the full nonlinear solutions to the governing equations.

The normal flow approximation for the perturbed bed of figure 3(*b*) is obtained from (5.5) and (5.6) by dropping terms of $O(\psi)$, $O(\epsilon)$ and the smaller order, i.e. backwater (inertia and pressure) and Reynolds stress terms:

$$0 = 1 - \frac{\left(u^2 + v^2\right)^{1/2}}{h}v, \tag{6.1}$$

$$0 = -ak\sin\phi - \frac{\left(u^2 + v^2\right)^{1/2}}{h}u. \tag{6.2}$$

The following perturbation expansion for small amplitude a is introduced to solve (5.7), (6.1), and (6.2) subject to the constraints (5.11):

$$u = au_1(y,\phi) + O\left(a^2\right), \tag{6.3a}$$

$$v = v_0(y) + av_1(y,\phi) + O\left(a^2\right), \tag{6.3b}$$

$$h = h_0(y) + ah_1(y,\phi) + O\left(a^2\right). \tag{6.3c}$$

Carrying out the solution, the base normal flow is found at lowest order, as

expected:

$$v_0 = y^{1/3}, \quad h_0 = y^{2/3}. \tag{6.4a,b}$$

At linear order in a, it is found that

$$v_1 = \tfrac{1}{6}k^2 y^{4/3}\cos\phi, \tag{6.5a}$$

$$h_1 = \tfrac{1}{3}k^2 y^{5/3}\cos\phi, \tag{6.5b}$$

$$u_1 = -y^{1/3}k\sin\phi. \tag{6.5c}$$

It is furthermore found from (5.13) that to linear order in a,

$$\tau_b = 1 + 2av_1 = 1 + a\tfrac{1}{3}k^2 y^{4/3}\cos\phi. \tag{6.6}$$

The reason for the failure of the normal flow approximation to select finite wavenumber can now be seen. From (6.6), it is apparent that τ_b is maximized in troughs, e.g. $\phi = 0$. The value of wavenumber k associated with the maximum trough value of τ_b is the one for which threshold condition would be reached in the shortest distance downstream of the divide. In the light of (2.3), this same wavenumber would be expected to cause the most rapid rate of erosion downstream of the threshold point. Maximizing the trough value of τ_b, however, yields the result $k = \infty$, or vanishing wavelength.

Whether viewed from the point of either classical linear stability analysis or the alternative threshold criterion offered here, the normal flow model combined with a purely erosional treatment of the topographic surface fails to select finite characteristic wavenumber. Equations (6.3)–(6.6) may likewise be used in the context of a transportational treatment of the topographic surface to yield the result of Smith & Bretherton (1972), in which again no finite characteristic wavelength is realized. The cause of the failure is evidently not rooted in the nature of the formulation of the Exner equation of sediment continuity, but rather in the normal flow approximation.

The normal flow approximation interestingly allows exact nonlinear solution independent of the magnitude of a. This solution sheds further light on the failure of the approximation. Let (q_x, q_y) denote the vector of water discharge per unit width, given by

$$(q_x, q_y) = (uh, vh). \tag{6.7}$$

Recalling that transverse phase $\phi = kx$, where both k and x are dimensionless, the equation of water continuity (5.7) can be written in the form

$$\frac{\partial q_x}{\partial x} + \frac{\partial q_y}{\partial y} = 1. \tag{6.8}$$

The momentum balance equations (6.1) and (6.2) of the normal flow can be used with (6.7) to obtain the result

$$\frac{q_y}{q_x} = \frac{v}{u} = -\frac{1}{ka\sin kx}. \tag{6.9}$$

Streamlines $y = y(x)$ for the overland flow can be obtained from (6.9);

$$\frac{\mathrm{d}y}{\mathrm{d}x} = -\frac{1}{ka\sin kx}. \tag{6.10}$$

This equation integrates to yield

$$y = -\frac{1}{2ak^2}\ln\left(\frac{1-\cos kx}{1+\cos kx}\right) + B_s. \tag{6.11}$$

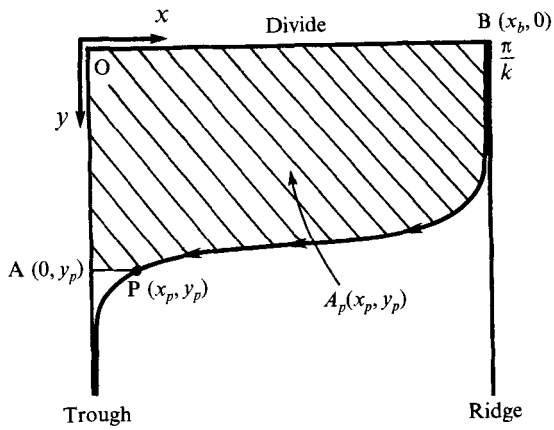

FIGURE 7. Illustration of a typical streamline from ridge to trough resulting from the nonlinear normal flow analysis.

The constant of integration B_s can be evaluated by considering the streamline passing through point (x_p, y_p) of figure 7. The streamline $y(x; x_p, y_p)$ passing through the point (x_p, y_p) is then found to take the form

$$y(x; x_p, y_p) = y_p + \frac{1}{2ak^2} \ln\left(\frac{1-\cos kx_p}{1+\cos kx_p}\right) - \frac{1}{2ak^2} \ln\left(\frac{1-\cos kx}{1+\cos kx}\right). \tag{6.12}$$

Now in general (6.8) integrates to yield

$$\iint_{A_p} \nabla \cdot \boldsymbol{q}\, \mathrm{d}A_p = \int_{S_p} \boldsymbol{q} \cdot \boldsymbol{n}\, \mathrm{d}S_p = A_p. \tag{6.13}$$

Here $\boldsymbol{q}$ denotes the vector (q_x, q_y), A_p denotes a given area, S_p denotes the closed curve surrounding this area, and $\boldsymbol{n}$ denotes a unit outward normal vector to this area. In figure 7, the area $A_p(x_p, y_p)$ is defined to be that enclosed by the curve AOBP, i.e. the divide, the line $x = 0$ corresponding to the trough passing through the origin, the streamline passing through point (x_p, y_p), and the line parallel to $y = 0$ connecting the trough to (x_p, y_p). Note that the streamline passing through (x_p, y_p) originates at point $(x_b, 0)$ where in accordance with (5.11) $0 < x_b < \pi/k$. Carrying out the indicated integrals of (6.13) in accordance with (5.11), it is found that

$$\int_0^{x_p} q_y(x, y_p)\, \mathrm{d}x = A_p, \tag{6.14a}$$

where

$$A_p(x_p, y_p) = x_p y_p + \int_{x_p}^{x_b} y(x; x_p, y_p)\, \mathrm{d}x. \tag{6.14b}$$

Here the parameter x_b can be evaluated from (6.12) to yield

$$x_b = \frac{1}{k} \cos^{-1}\left\{ \frac{2}{1+\exp\left[2ak^2 y_p + \ln\left(\frac{1-\cos kx_p}{1+\cos kx_p}\right)\right]} - 1 \right\}. \tag{6.15}$$

Taking the derivative of (6.14) with respect to x, it is found that

$$q_y(x_p, y_p) = \frac{x_b - x_p}{ak \sin kx_p}. \tag{6.16}$$

The result of essential importance can now be obtained. Consider the streamwise discharge at the trough $q_y(0, y_p)$ obtained by setting $x_p = 0$ in (6.16). It is seen from (6.15) and (6.16) that $q_y(0, y_p) = 0$ for $y_p = 0$, i.e. at the divide, but suddenly jumps to infinity for any $y_p > 0$. That is, the trough discharge jumps to infinity if any flow at all is allowed to gather from the surrounding basin. In the normal flow approximation, there is nothing to stop this overconcentration of flow. Loewenherz (1991) attempted to resolve this problem by adding an *ad hoc* 'smearing function'. Here the resolution of the issue will be sought with the aid of the terms neglected in making the normal flow approximation.

7. Renormalization

In §6, it was shown that the normal flow approximation results in the failure of finite wavelength selection both at the linear and nonlinear levels. This notwithstanding, it can be expected that both the backwater and Reynolds stress terms neglected in the normal flow approximation play a role in preventing infinite concentration of flow for basins of finite dimension. For example, the concentration of flow in the troughs should elevate depth there, creating a ridgeward pressure gradient that would act to resist further concentration. In addition, the transverse Reynolds stress is associated with turbulent eddy viscosity that should also act to prevent overconcentration especially for larger values of k (smaller wavelength). The small parameters ψ and ϵ can be used as measures of backwater and Reynolds effects, respectively.

In order to see this, it is useful to renormalize (5.5)–(5.7) as follows:

$$x^* = \frac{x}{\psi}, \quad k^* = \psi k. \tag{7.1a,b}$$

The meaning of this renormalization can be clarified by reverting to dimensioned parameters, which are hereby denoted with the subscript d in order to distinguish them from dimensionless parameters from which the hats have been removed. From (7.1), (4.11) and (5.1), it is found that

$$x_d = \frac{H_{th}}{S} x^*, \quad k_d = \frac{S}{H_{th}} k^*. \tag{7.2a,b}$$

The non-dimensionlization of §5, however, corresponds to

$$k_d = \frac{1}{L_{th}} k. \tag{7.3}$$

While order-one values of k correspond to $k_d \sim 1/L_{th}$, order-one values of k^* correspond to the estimate $k_d \sim S/H_{th}$. Insofar as $H_{th}/(SL_{th}) = \psi \ll 1$, it is seen that (7.1) allows for a reselection of large wavenumbers, i.e. transverse wavelengths that are short compared to L_{th}. It is shown below that this renormalization provides the key to the resolution of the problem posed by the failure of the naive analysis of §6 to select finite wavelength.

Substituting (7.1) into (5.5)–(5.7) and (5.11), it is found that

$$F^2\left(k^* u\frac{\partial v}{\partial \phi}+\psi v\frac{\partial v}{\partial y}\right)+\psi\frac{\partial h}{\partial y}=1-\frac{(u^2+v^2)^{1/2}}{h}v + \epsilon\left[k^{*2}\frac{\partial}{\partial \phi}\left(\chi\frac{\partial v}{\partial \phi}\right)+\psi^2\frac{\partial}{\partial y}\left(\chi\frac{\partial v}{\partial y}\right)\right], \tag{7.4}$$

$$F^2\left(k^* u\frac{\partial u}{\partial \phi}+\psi v\frac{\partial u}{\partial y}\right)+k^*\frac{\partial h}{\partial \phi}=-ak^*\sin\phi-\frac{(u^2+v^2)^{1/2}}{h}u + \epsilon\left[k^{*2}\frac{\partial}{\partial \phi}\left(\chi\frac{\partial u}{\partial \phi}\right)+\psi^2\frac{\partial}{\partial y}\left(\chi\frac{\partial u}{\partial y}\right)\right], \tag{7.5}$$

$$k^*\frac{\partial uh}{\partial \phi}+\psi\frac{\partial vh}{\partial y}=\psi, \tag{7.6}$$

$$vh\big|_{y=0}=0, \tag{7.7a}$$

$$u\big|_{\phi=0,\pm\pi,\cdots}=0, \tag{7.7b}$$

$$\frac{\mathrm{d}}{\mathrm{d}y}\int_{-\pi}^{\pi}vh\,\mathrm{d}\phi=2\pi. \tag{7.7c}$$

It is seen from these equations that the parameters ψ and ϵ scale the streamwise backwater terms and the transverse Reynolds stress terms, respectively.

It is of value to view the base flow in terms of the renormalized parameters. This is obtained from the above equations by setting $a=0$, from which it can be found that $u=0, v=v_0(y)$, and $h=h_0(y)$. Equations (7.4) and (7.6) then reduce to

$$1-\frac{v_0^2}{h_0}=-\psi\left[F^2 v_0\frac{\mathrm{d}v_0}{\mathrm{d}y}+\frac{\mathrm{d}h_0}{\mathrm{d}y}-\psi\epsilon\frac{\mathrm{d}}{\mathrm{d}y}\left(v_0 h_0\frac{\mathrm{d}v_0}{\mathrm{d}y}\right)\right], \tag{7.8}$$

$$\frac{\mathrm{d}v_0}{\mathrm{d}y}=1. \tag{7.9}$$

The base normal flow is thus obtained strictly in the limit as $\psi\to 0$, for which both streamwise backwater and Reynolds stress terms are seen to vanish. In analogy to (6.4), the base normal solution is found to be

$$v_{bn}=y^{1/3},\quad h_{bn}=y^{2/3}. \tag{7.10a,b}$$

Imposition of (5.14) leads to the expected condition for the threshold of motion in the case of the base normal flow;

$$\ell=1. \tag{7.11}$$

8. Solution

A perturbation technique using a,ψ, and ϵ as small parameters is used here to solve (7.4)–(7.7). While ψ and ϵ are characteristic parameters of each configuration, a is chosen to be arbitrarily small. The following composite expansions are introduced in order to perform a linear analysis in a:

$$u=au_1(y,\phi), \tag{8.1a}$$

$$v = v_0(y) + a v_1(y, \phi), \tag{8.1b}$$

$$h = h_0(y) + a h_1(y, \phi), \tag{8.1c}$$

where

$$v_0(y) = v_{000}(y) + \psi v_{010}(y) + \epsilon v_{001}(y) + \psi^2 v_{020}(y) + \psi\epsilon v_{011}(y) + \epsilon^2 v_{002}(y) + \cdots, \tag{8.2a}$$

$$h_0(y) = h_{000}(y) + \psi h_{010}(y) + \epsilon h_{001}(y) + \psi^2 h_{020}(y) + \psi\epsilon h_{011}(y) + \epsilon^2 h_{002}(y) + \cdots. \tag{8.2b}$$

and

$$u_1(y, \phi) = u_{100}(y, \phi) + \psi u_{110}(y, \phi) + \epsilon u_{101}(y, \phi) + \cdots, \tag{8.3a}$$

$$v_1(y, \phi) = v_{100}(y, \phi) + \psi v_{110}(y, \phi) + \epsilon v_{101}(y, \phi) + \cdots, \tag{8.3b}$$

$$h_1(y, \phi) = h_{100}(y, \phi) + \psi h_{110}(y, \phi) + \epsilon h_{101}(y, \phi) + \cdots. \tag{8.3c}$$

Note that the subscript 0 in (8.1) and (8.2) corresponds to the base flow, i.e. the limit as a tends to zero. Likewise, the subscript 000 in (8.2) corresponds to the base normal flow, i.e. the limit as a, ψ, and ϵ all tend to zero. A constraint on the validity of the expansion is that $a^2 \ll \max(\psi^2, \epsilon^2)$, a condition that is consistent with a linear analysis for infinitesimal a.

The terms of the base solution in (8.1) and (8.2) that differ from the base normal solution are independent of the perturbation, and thus are not dependent upon x or k^*. As a result, they simply alter the position at which the base flow attains the threshold condition by a constant value about the base normal value $\ell = 1$, and play no role in determining the selection of characteristic wavenumber. For this reason, it turns out to be unnecessary to carry the expansion of the base flow to $O(a)$.

Substituting (8.1)–(8.3) into (7.4)–(7.7) and carrying out the solution, it is found that

$$v_0 = y^{1/3} - \psi \frac{F^2 + 2}{9} + O(\psi^2, \epsilon^2), \tag{8.4a}$$

$$h_0 = y^{2/3} + \psi \frac{F^2 + 2}{9} y^{1/3} + O(\psi^2, \epsilon^2), \tag{8.4b}$$

and

$$u_1 = -\psi \frac{y^{-4/3}}{2k^*} \sin\phi + O(\psi^2, \epsilon^2), \tag{8.5a}$$

$$v_1 = \left[\frac{1}{2} y^{-1/3} - \psi\left(\frac{y^{-2}}{4k^{*2}} + \frac{F^2 + 2}{9} y^{-1/3}\right) - \epsilon \frac{k^{*2}}{4} y\right] \cos\phi + O(\psi^2, \epsilon^2), \tag{8.5b}$$

$$h_1 = \left[1 - \psi \frac{y^{-5/3}}{2k^{*2}}\right] \cos\phi + O(\psi^2, \epsilon^2). \tag{8.5c}$$

The parameter $\Delta\ell$ defined by (5.12) can be determined by substituting the above expressions into (5.14) and expanding. This results in

$$\Delta\ell = \Delta\ell_0 + a\Delta\ell_1, \tag{8.6}$$

where

$$\Delta\ell_0 = -\psi \frac{F^2 + 2}{3} + O(\psi^2, \epsilon^2) \tag{8.7}$$

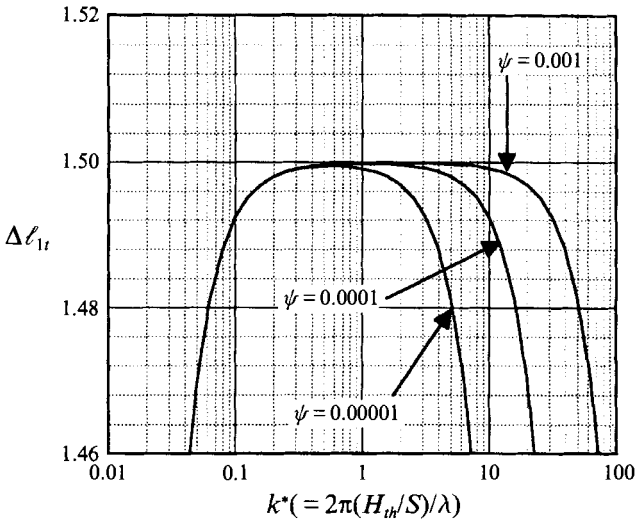

FIGURE 8. Plot of $\Delta\ell_1$ versus k^* for the case $F = 0.05$ and $\epsilon = 0.0001$. Curves are shown for $\psi = 0.00001, 0.0001, 0.001$.

and

$$\Delta\ell_1 = 3\left[\frac{1}{2} - \psi\left(\frac{1}{4k^{*2}} + \frac{F^2+2}{9}\right) - \epsilon\frac{k^{*2}}{4} + O\left(\psi^2, \epsilon^2\right)\right]\cos\phi. \tag{8.8}$$

In figure 8, the trough value $\Delta\ell_t$ corresponding to the expression $\Delta\ell$ evaluated at $\phi = 0$ is plotted versus wavenumber k^* for the case $F = 0.5$, $\epsilon = 0.0001$, and the values $\psi = 0.00001$, 0.0001, and 0.001. The curves demonstrate the existence of a characteristic wavenumber k_c^* at which $\Delta\ell_t$ is maximized. This results from a combination of backwater and Reynolds stress effects. In (8.8), the effect of ψ upon $\Delta\ell_t$ is to favour larger values of k^* (smaller wavenumber), and the effect of ϵ is to favour smaller values of k^* (larger wavenumber).

An expression for characteristic wavenumber can now be derived with the use of (2.4). A perusal of (8.6)–(8.8) indicates that $\Delta\ell_t = \Delta\ell|_{\phi=0}$ is maximized when $\Delta\ell_{1t}$ is maximized, where $\Delta\ell_{1t}$ is obtained from (8.8) by setting $\phi = 0$:

$$\Delta\ell_{1t} = 3\left[\frac{1}{2} - \psi\left(\frac{1}{4k^{*2}} + \frac{F^2+2}{9}\right) - \epsilon\frac{k^{*2}}{4} + O\left(\psi^2, \epsilon^2\right)\right]. \tag{8.9}$$

Performing the maximization, it is found that characteristic wavenumber k_c^* is given by the simple expression

$$k_c^* = \left(\frac{\psi}{\epsilon}\right)^{1/4}. \tag{8.10}$$

This relation can be reduced with the aid of (3.5), (3.6), (4.8), (4.9), (4.10), (4.11), (5.1), and (5.9) the following form for dimensioned characteristic wavelength:

$$\lambda_{dc} = \frac{2\pi}{g}\left(\frac{\alpha}{C_f}\right)^{1/4} u_{*th}^{9/4} S^{-5/4} I^{-1/4}. \tag{8.11}$$

In the above relation, λ_{dc} denotes the dimensioned characteristic wavelength, and the dimensioned critical shear velocity u_{*th} is defined by the relation

$$\rho u_{*th}^2 = \tau_{th}. \tag{8.12}$$

9. Discussion and conclusions

It is of value to apply (8.11) to a specific case. To this end, the coefficient α in the relation (3.5) is evaluated with the aid of (3.7), i.e. set equal to 0.2. The friction coefficient C_f for overland sheet flow can be expected to be rather higher than that for channel flow; here a value of 0.01 is assumed. Various estimates are available for the critical shear stress τ_{th}, or alternatively critical shear velocity u_{*th}, for cohesive sediments in general (e.g. Vanoni 1975; Raudkivi 1976) and for vegetated soil surfaces in particular (e.g. Dietrich *et al.* 1993). These values typically range from 0.02 to 0.2 m s^{-1}. Here a value of u_{*th} of 0.1 m s^{-1} is adopted as representative.

The present analysis cannot predict the fine structure of the drainage basins of figures 1 and 2 as they appear in their present, fully dissected states. Rather, it might be thought to apply to some antecedent undissected state consisting of a flat but tilted surface with a much lower slope than that prevailing at the present channel heads shown in figures 1 and 2. With this in mind, a sample value of slope S of 0.01 is used here. In addition, a fairly intense rainfall of 100 mm hr^{-1} is assumed.

Used in conjunction with (4.8)–(4.10), the above values yield the following predictions for the base flow: a threshold flow velocity V_{th} of 1.00 m s^{-1}, a threshold depth H_{th} of 0.102 m, and a distance L_{th} from divide to the first point at which threshold conditions are reached of 3670 m. The parameters ψ and ϵ are found to take the value 2.78×10^{-3} and 2.00×10^{-4} respectively. As expected, both these values are small.

Equation (8.11) yields a predicted value of characteristic wavelength λ_{dc} of 33.1 m. This value is somewhat smaller than, but of the same order of magnitude as, the spacing between channel heads found in the Hay Press and Sausalito tributaries of Tennessee Valley, California by Montgomery & Dietrich (1989), and in the basins at Rock Creek, Oregon, Southern Sierra, California, and San Dimas, California studied by Dietrich & Dunne (1993). This encouraging result nevertheless requires some interpretation.

Figure 9 illustrates how the flat but tilted plateau assumed here might evolve into a mature drainage basin. Channelization first begins rather far down the slope, with a spacing that might be predicted by the present model. The channel heads then migrate upstream by the process of head cutting at the same time as they incise. The process of incision can be expected to be subject to the controls of regolith formation, tectonic uplift or subsidence, and climate. As it progresses, some incipient basins can be expected to capture their neighbours, so that basin spacing thins out. On the other hand, as the original tilted but flat plateau evolves toward an overall upward concave terrain with steepened headwaters, lateral sub-basins can be expected to evolve. As it reaches some degree of morphological maturity, the basin can be expected to look quite different from the hypothesized original configuration of figure 9. This notwithstanding, it is reasonable to expect that the finest scale of channel spacing associated with the final state scales at least approximately with that predicted from the present analysis.

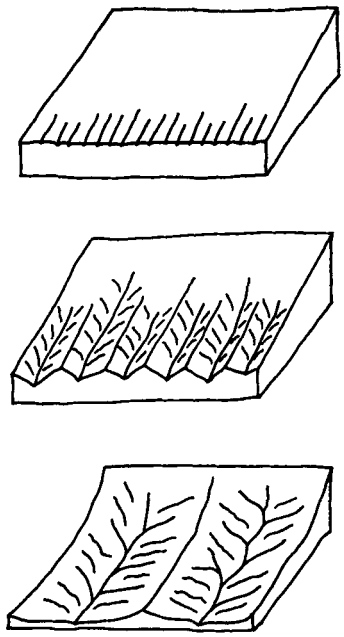

FIGURE 9. Schematic diagram illustrating the hypothesized pattern of evolution from the state of incipient channelization discribed here to a more mature geomorphic state.

The full evolution to a geomorphically mature state cannot be predicted with the present model, which does not attempt to include the complexities of the models of Willgoose *et al.* (1989, 1991 *a*, *b*) and Howard (1994). For example, the rounding of ridges between adjacent basins and along divides is thought to be associated with a diffusive mechanism associated with rainsplash, a process that is not even considered here. The suggestion is rather that the flow model presented here, which is capable of predicting a characteristic scale associated with incipient channelization, is probably a better place to start in constructing a full model of drainage basin evolution than the normal flow model. The incorporation of some version of the flow model presented here into the more general framework of Howard (1994), for example, might be expected to lead to results of considerable interest.

The implication is that the most appropriate avenue for further progress with the model involves numerical computations. Indeed, the present analysis could have been performed completely by means of a full numerical treatment of two-dimensional shallow water flow over a corrugated bed. Such an analysis would have obscured, however, the mechanistic basis for wavelength selection described here.

Several discussions with William Dietrich proved crucial to the formulation of the present model. Discussions with Alan Howard, who made a considerable body of unpublished information available to us, James Kirchner and Garry Willgoose are also gratefully acknowledged. James Kirchner piloted the airplane from which the photograph of figure 2 was taken. This research was funded by the National Science Foundation (grant no. CTS-9207882) and the Graduate School of the University of Minnesota (grant-in-aid of research, artistry and scholarship).

REFERENCES

ABRAHAMS, A. D. 1984 Channel networks: a geomorphological perspective. *Wat. Resources Res.* **20**, 161–168.

ARIATHURAI, R. & ARULANANDAN, K. 1978 Erosion rates of cohesive soils. *J. Hydraul. Div., ASCE* **104**, 279–283.

BLONDEAUX, P. & SEMINARA, G. 1985 A unified bar-bend theory of river meanders. *J. Fluid Mech.* **157**, 449–470.

COLOMBINI, M., SEMINARA, G. & TUBINO, M. 1987 Finite-amplitude alternate bars. *J. Fluid Mech.* **181**, 213–232.

DIETRICH, W. E. & DUNNE, T. 1993 The channel head. In *Channel Networks Hydrology* (ed. K. Berlin, & M. J. Kirkby), pp. 175–219. Wiley.

DIETRICH, W. E., WILSON, C. J., MONTGOMERY, D. R. & MCLEAN, J. 1993 Analysis of erosion thresholds, channel networks, and landscape morphology using a digital terrain model. *J. Geol.* **101**, 259–278.

ENGELUND, F. A. 1970 Instability of erodible beds. *J. Fluid Mech.* **42**, 225–244.

ENGELUND, F. A. & SKOVGAARD, O. 1973 On the origin of meandering and brading in alluvial streams. *J. Fluid Mech.* **57**, 289–302.

FISCHER, H. B., LIST, J. E., KOH, R. C. Y., IMBERGER, J. & BROOKS, N. H. 1979 *Mixing in Inland and Coastal Waters.* Academic.

FREDSOE, J. 1974 On the development of dunes in erodible beds. *J. Fluid Mech.* **64**, 1–16.

FREDSOE, J. 1978 Meandering and braiding of rivers. *J. Fluid Mech.* **84**, 609–624.

HORTON, R. E. 1945 Erosional development of streams and their drainage basins; hydrophysical approach to quantitative morphology. *Geol. Soc. Am. Bull.* **56**, 275–370.

HOWARD, A. D. 1990 Theoretical model of optimal drainage networks. *Wat. Resources Res.* **26**, 2107–2117.

HOWARD, A. D. 1994 A detachment-limited model of drainage basin evolution. *Wat. Resources Res.* **30**, 2261–2285.

IKEDA, S. & IZUMI, N. 1991 Stable channel cross sections of straight sand rivers. *Wat. Resources Res.* **27**, 2429–2438.

IKEDA, S., PARKER, G. & SAWAI, K. 1981 Bend theory of river meanders. Part 1. Linear development. *J. Fluid Mech.* **112**, 363–377.

IZUMI, N. 1993 Channelization and drainage basin formation in cohesive soils. PhD thesis, University of Minnesota.

LOEWENHERZ, D. S. 1991 Stability and the initiation of channelized surface drainage: a reassessment of the short wavelength limit. *J. Geophys. Res.* **96**, 8453–8464.

LUKE, J. 1974 Special solutions for nonlinear erosion problems. *J. Geophys. Res.* **79**, 4035–4040.

MEINHARDT, H. A. 1982 *Models of Biological Pattern Formation.* Academic.

MONTGOMERY, D. R. & DIETRICH, W. E. 1989 Source area, drainage density and channel initiation. *Wat. Resources Res.* **25**, 1907–1918.

PARKER, G. 1976 On the cause and characteristic scales of meandering and braiding in rivers. *J. Fluid Mech.* **76**, 457–480.

PARKER, G. 1978 Self-formed straight rivers with equilibrium banks and mobile bed. Part 1. The sand-silt river. *J. Fluid Mech.* **89**, 109–125.

PARTHENIADES, E. 1965 Erosion and deposition of cohesive soils. *J. Hydraul. Engng, ASCE* **91**, 105–139.

RAUDKIVI, A. J. 1976 *Loose Boundary Hydraulics,* 2nd Edn. Pergamon.

RICHARDS, K. J. 1980 The formation of ripples and dunes on an erodible bed. *J. Fluid Mech.* **99**, 597–618.

RODI, W. 1980 *Turbulence Models and their Applications in Hydraulics.* IAHR.

ROTH, G. & SICCARDI, F. 1989 Hydrodynamic description of the erosional development of drainage patterns. *Wat. Resources Res.* **25**, 319–332.

SAWAI, K., ASHIDA, K. & IMAMOTO, H. 1986 Stream network evolution and sediment yield on a bare slope. In *Proc. 3rd Intl Symp. on River Sedimentation* (ed. S. Y. Wang). University of Mississippi.

SCHIELEN, R., DOELMAN, A., & SWART, H. E. DE 1993 On the nonlinear dynamics of free bars in straight channels. *J. Fluid Mech.* **252**, 325–356.

SHEN, H. W. & LI, R. M. 1973 Rainfall effect on sheet flow over smooth surface. *J. Hydraul. Engng, ASCE* **99**, 771–792.

SMITH, J. D. 1970 Stability of a sand bed subjected to shear flow at low Froude Number. *J. Geophys. Res.* **75**, 5928–5940.

SMITH, T. & BRETHERTON, F. B. 1972 Stability and the conservation of mass in drainage basin evolution. *Wat. Resources Res.* **8**, 1506–1529.

STRAHLER, A. N. 1958 Dimensional analysis applied to fluvially eroded landforms. *Bull. Geol. Soc. Am.* **69**, 279–300.

TUBINO, M. & SEMINARA, G. 1990 Free-forced interactions in developing meanders and suppression of free bars. *J. Fluid Mech.* **214**, 131–159.

VANONI, V. A. (ED.) 1975 *Sedimentation Engineering*. American Society of Civil Engineers.

WILLGOOSE, G., BRAS, R. & RODRIGUEZ-ITURBE, I. 1989 A physically based channel network and catchment model. *Rep.* 322, Ralph Parsons Laboratory, Department of Civil Engineering, Massachusetts Institute of Technology.

WILLGOOSE, G., BRAS, R. & RODRIGUEZ-ITURBE, I. 1991 *a* A coupled channel network growth and hillslope evolution model. 1. Theory. *Wat. Resources Res.* **27**, 1671–1684.

WILLGOOSE, G., BRAS, R. & RODRIGUEZ-ITURBE, I. 1991 *b* A coupled channel network growth and hillslope evolution model. 2. Nondimensionalization and applications. *Wat. Resources Res.* **27**, 1685–1696.

YOON, Y. N. & WENZEL., H. G., JR. 1971 Mechanics of sheet flow under simulated rainfall. *J. Hydraul. Engng, ASCE* **97**, 1367–1386.